

AN ABSTRACT OF THE THESIS OF

Insoo Kang for the degree of Master of Science in Civil Engineering presented on July 10, 2020.

Title: On the use of GNSS-derived PWV for Predicting the Path of Typhoon: Case Studies for Soulik and Kongrey in 2018

Abstract approved: _____

Jihye Park

A typhoon is a highly destructive weather event, causing severe damage and losses to the economy and lives. The impacts of typhoons can be mitigated by adequately predicting their path in advance. The progress of a typhoon can be investigated by analyzing the significant changes in Precipitable Water Vapor (PWV) in a given region. Global Navigation Satellite Systems (GNSS) have been utilized to monitor the changes in PWV since GNSS meteorology was introduced in the early 1990s. In this study, PWV variations of two typhoons, Soulik and Kongrey in 2018, are investigated based on GNSS derived PWV (GNSS-PWV). The variations in GNSS-PWV are used for predicting the typhoon path, provided that the movement direction of PWV corresponds to that of a typhoon. In the study area, GNSS stations are densely distributed like an array so that the array enables to monitor the variations of PWV over the region more sensibly than a conventional PWV monitoring method, which is the radiosonde based PWV observations (RS-PWV). Comparing the results of GNSS-PWV to the RS-PWV, GNSS-PWV is proved to be comparable and even provides better spatiotemporal resolution. It should be noted that the GNSS-PWV is investigated with meteorological parameters together during a typhoon event. The pattern of GNSS-PWV showed the opposite pattern of air pressure, which is one of the essential factors in conventional typhoon forecast methods. As the GNSS-PWV and the pressure are strongly correlated, this study only focused on the GNSS-PWV for analyzing the meteorological variations and predicting the path of typhoons. To predict the

typhoon's subsequent location, the research proposes the concept of Predicted Location of Typhoon (PLT). PLT is calculated as follows: 1) estimated all the GNSS-PWV in the study area during a typhoon event. 2) The top five GNSS stations showing the highest PWV are selected. 3) The 2-dimension mean position of them is calculated. 4) This position indicates the PLT corresponding to the process of the typhoon. The research model predicted a typhoon's subsequent location approximately 5 hours in advance with an average distance discrepancy of 14 km in two experiments. When the typhoon approaches the landfall point, the research model managed to predict the landfall point, approximately 5.3 hours in advance, with an average distance discrepancy from the actual path of 13.19 km in two experiments. Although the proposed method used only GNSS-PWV using existing GNSS stations, it still yielded comparable results of typhoon paths, comparing those issued by Korea Meteorological Administration (KMA), who considerably applied the conventional and certified method for forecasts. These results imply that GNSS-PWV is promising for the prediction of the typhoon path seamlessly in a cost-effective and environmentally friendly manner, and it can be used for the supplementary information for the current typhoon forecast.

Keywords: GNSS meteorology, PWV, Typhoon, Predicted Location of Typhoon

©Copyright by Insoo Kang

July 10, 2020

All Rights Reserved

On the use of GNSS-derived PWV for Predicting the Path of Typhoon: Case Studies for Soulik
and Kongrey in 2018

by
Insoo Kang

A THESIS

submitted to

Oregon State University

in partial fulfillment of
the requirements for the
degree of

Master of Science

Presented July 10, 2020
Commencement June 2021

Master of Science thesis of Insoo Kang presented on July 10, 2020.

APPROVED:

Major Professor, representing Civil Engineering

Head of the School of Civil and Construction Engineering

Dean of the Graduate School

I understand that my thesis will become part of the permanent collection of Oregon State University libraries. My signature below authorizes release of my thesis to any reader upon request.

Insoo Kang, Author

ACKNOWLEDGEMENTS

First and foremost, I would like to express my sincere gratitude to my beloved country, the Republic of South Korea, and especially to the Republic of Korea Army for letting me study in the United States.

I would also like to thank my supervisor Dr. Jihye Park, whose advice, support, and encouragement have been invaluable throughout this study. And I would also like to thank my whole committee, including Dr. Mike Olsen, Dr. Chris Parrish, and Dr. Yue Zhang for generously sparing their time to offer me invaluable comments toward improving my work.

Thank you to all my fellow geomatics graduate students. I will never forget the sleepless nights we spent working together, and for all the fun we have had.

Moreover, I would also like to express my deep gratitude to my fellow soldiers who devote themselves to the defense of the Republic of Korea.

Finally, nobody has been more important to me than my family in the pursuit of this study. Their unconditional trust and love have always lifted me.

TABLE OF CONTENTS

	<u>Page</u>
1. INTRODUCTION.....	1
2.GNSS METEOROLOGY	3
3.PREDICTION OF TYPHOON PATH BASED ON GNSS-PWV.....	5
3.1 Study Site Description.....	5
3.2 Computation of GNSS-PWV	8
3.3 Prediction Technique Based on PWV	11
4. EXPERIMENT RESULTS AND VALIDATION.....	16
4.1 Soulik	17
4.2 Kongrey.....	21
4.3 Comparison	23
5. SUMMARY AND CONCLUSION	25
BIBLIOGRAPHY	28

LIST OF FIGURES

<u>Figure</u>	<u>Page</u>
Fig. 1. The distribution of GNSS stations, RS stations and MT stations in South Korea..	6
Fig. 2. The forecasted paths of Soulik (left) and Kongrey (right) by KMA..	8
Fig. 3. The comparison between GNSS-PWV and RS-PWV in Jeju, during the whole cycle of each typhoon.	10
Fig. 4. The time series of PWV, pressure, temperature, and precipitation in Jeju during the whole cycle of Kongrey.	11
Fig. 5. Determination of PLT based on GNSS-PWV.	13
Fig. 6. The scatter plots depict the recordings of PWVs for individual stations sorted in descending order.	15
Fig. 7. The result of the research model during the Soulik event.	18
Fig. 8.	19
Fig. 9. The result of the research model during Kongrey	22
Fig. 10. Comparison of the forecasts.	25

LIST OF TABLES

<u>Table</u>	<u>Page</u>
Table 1. The comparison between the radiosonde and GNSS meteorology	3
Table 2. Typhoon Classification in South Korea	7
Table 3. The statistical comparison, PLT versus the rest stations	14
Table 4. Soulik status and the results of the research model.	17
Table 5. The result of the research model for the Soulik case.	20
Table 6. Kongrey Status and the results of the model.....	21
Table 7. The result of the proposed model for the Kongrey case.	23
Table 8. The comparison of the research model and the official forecast in each case.	24

1. INTRODUCTION

Atmospheric water vapor plays a critical role in the hydrologic cycle, especially for the development of many atmospheric storm events (Bordi et al. 2014). Measuring the distribution of water vapor in the atmosphere leads to accurate forecasts of severe weather phenomena and contributes to a better understanding of climate change (Bevis et al. 1992, Yao et al. 2017). Of the extreme weather events, a typhoon, causing torrential rains and associated storm surges (Zhao et al. 2018, Lu et al. 2019), is formed with a great deal of water vapor. A tropical cyclone is a common severe event and referred to as a typhoon when the event originates in the Northwest Pacific, and as a hurricane when it originates in the North Atlantic, central North Pacific, and eastern North Pacific (National Hurricane Center 2020). As the progression of a tropical cyclone can be investigated by means of monitoring the changes of water vapor over a region (Yoshikane& Kimura 2005), many studies have focused on monitoring water vapor for forecasting (Weng et al. 2016, Zhao et al. 2019).

Currently, one of the dominant methods for measuring atmospheric water vapor relies on the use of a direct measurement sensor, the radiosonde. The radiosonde is a weather-balloon-launched instrument package that directly measures not only the atmospheric water vapor but also meteorological upper air data—such as temperature, pressure, humidity. It has been considered among the most reliable and handy atmospheric measuring tool and has facilitated a significant amount of research on the atmosphere for over seven decades (Wang& Zhang 2008).

Despite these advantages, the radiosonde may not provide sufficient spatiotemporal resolution (Elliott& Gaffen 1991, Li et al. 2003, Soden et al. 2004, Wang& Zhang 2008). Its relatively high cost restricts the temporal resolution—it is used only two to four times a day. The sensor performance is hindered in cold and dry conditions. Additionally, it can fly horizontally 350 km at the most, i.e., the device may provide poor horizontal accuracy, and it is rarely retrieved. As a result, used radiosondes cause significant environmental damage, given that there are over 900 hundred radiosonde stations in the world.

On the other hand, Global Navigation Satellite System (GNSS) has been used as another measuring tool of water vapor in the atmosphere. GNSS is widely used in different applications, especially determining a 3-dimension position with high accuracy. To obtain highly accurate solutions, errors on the GNSS signals should be appropriately mitigated. GNSS signals, for instance, are delayed nearly proportional to the quantity of the integrated water vapor along with their path (Hogg et al. 1981, Askne& Nordius 1987). In other words, the error on the GNSS signals caused by the atmospheric effect can be converted to the total amount of the atmospheric water vapor. Based on this relationship, the possibility of detecting water vapor with GNSS has been raised, which is called GNSS meteorology (Bevis et al. 1992). When the total quantity of the water vapor is expressed as the height of an equivalent column of liquid water overlaying a point on the Earth's surface, it is defined as Precipitable Water Vapor (PWV) (Bevis et al. 1994), i.e., PWV can be used to reflect the variations in the atmospheric water vapor.

Unlike the case of radiosonde, which provides poor temporal and spatial resolution and hard to keep up for multiple uses, GNSS can provide the PWV readings in a seamless and cost-effective manner in all weather conditions, which is a significant advantage of GNSS over the radiosonde. Moreover, there are more GNSS stations in the world than the radiosonde stations, which implies that GNSS meteorology provides more improved spatiotemporal resolution. For instance, when GNSS-PWV is put into Numerical Weather Prediction models, moisture and rainfall forecasts (Gutman& Benjamin 2001), intense rainfall (Kanda 2000), and tropical cyclone intensity forecasts (Shoji et al. 2011) have been improved. Furthermore, it was reported that GNSS-PWV had the same or higher accuracy than the PWV observed by the radiosonde (RS-PWV) (Shoji et al. 2004). Wang and Zhang (2008) indicated that GNSS-PWV was useful for identifying and quantifying several kinds of systematic errors in the RS-PWV. The overall comparison between the radiosonde and GNSS-meteorology is addressed in Table 1.

This study explores the feasibility of predicting the movements of a typhoon using the variations of GNSS-PWV and investigates the efficacy of that method. The proposed method was applied to two typhoons, which served as case studies. Two questions guided the investigation: 1) how early in advance the research method was able to predict points in a typhoon's trajectory, and 2) how accurate the research method's prediction was (i.e., how much error (in kilometers) the

method had). Finally, the study examined the relationship between GNSS-PWV and atmospheric parameters (e.g., precipitation, temperature, and air pressure) to better understand the factors that inform typhoon predictions.

Table 1. The comparison between the radiosonde and GNSS meteorology

	Radiosonde	GNSS Meteorology
Operational manner	Balloon-based	Station-based
Spatial resolution (the number of stations in South Korea)	7	186
Temporal resolution	2 – 4 times a day	All the time
Cost	≈ \$150 each	≈ \$5,000 (hardware)
Measurement data	Upper air data (water vapor, temperature, pressure, humidity.)	Water vapor
Characteristics	<ul style="list-style-type: none"> - A long history - Poor horizontal resolution - Harmful impact on the environment 	<ul style="list-style-type: none"> - More reliable data for the launch site - Less harmful to the environment

2. GNSS METEOROLOGY

GNSS has been widely utilized for a variety of applications, mainly with its primary purpose of positioning, navigation, and timing (PNT). To ensure the accuracy of the PNT, GNSS scientists have exerted considerable effort to remove or mitigate GNSS error sources, such as ephemeris data, satellite clock, ionosphere, troposphere, multipath, receiver measurement (Hofmann-Wellenhof et al. 2007). Of these error sources, total tropospheric delay (TD) occurs in the troposphere. It is caused by mainly two factors—the hydrostatic component caused by the refractivity of dry gases and the wet component caused by the refractivity of water vapor, respectively (Davis et al. 1985). This relationship is expressed as below (Hofmann-Wellenhof et al. 2007).

$$TD = 10^{-6} \int N_d^{Trop} ds + 10^{-6} \int N_w^{Trop} ds \quad (1)$$

where N_d^{Trop} is the dry part results from the dry (hydrostatic) atmosphere and N_w^{Trop} is the wet part results from the water vapor. If the TD in slant path delay can be projected onto the zenith direction, it yields Zenith Tropospheric Delay (ZTD) by using a mapping function which depends on the meteorological parameters and the elevation angle of the satellite (Davis et al. 1985).

$$ZTD = ZHD \cdot m_h + ZWD \cdot m_w \quad (2)$$

where m_h and m_w are the hydrostatic and wet mapping functions, respectively. Zenith hydrostatic delay (ZHD) is the signal delay due to the dry gas, and zenith wet delay (ZWD) is the signal day due to the wet components in the atmosphere. ZHD is well-estimated by empirical models with surface meteorological data, having an error of about 1 % of actual delay (Seeber 2008). In contrast, estimating ZWD is challenging directly due to the heterogeneity of water vapor. Thus, ZWD is estimated by extracting ZHD from ZTD in eq. (2). ZHD has an average magnitude of about 2.3 m at sea level, whereas ZWD can range from a few millimeters in very arid conditions to more than 350 mm in very humid conditions (Duan et al. 1996).

Then, the ZWD can be converted into PWV through a conversion factor (Askne& Nordius 1987) :

$$PWV = \Pi \cdot ZWD \quad (3)$$

where the Π is a dimensionless constant of proportionality, which is given by

$$\Pi = \frac{10^6}{\rho R_v \left[\left(\frac{k_3}{T_m} \right) + k'_2 \right]} \quad (4)$$

where ρ is the density of water (998.00897 [kg/m⁻³]), and R_v is the specific volume of water vapor (461.51 [J/ (kg· K)]), and $k'_2 = 17 \pm 10$ [K/hPa] and $k_3 = (3.82 \pm 0.04) \times 10^5$ [K²/hPa] were applied, respectively (Davis et al. 1985). T_m is the empirical weighted mean temperature of

troposphere (K), which can be estimated using measurements of surface temperature (Bevis et al. 1992) or numerical weather models (Bevis et al. 1994).

$$T_m = 70.2 + 0.72 \cdot T_s \quad (5)$$

where T_s is the surface temperature. The conversion of ZWD into PWV in eq. (3) assumes that ZWD is mainly due to water vapor and that liquid and ice hardly play a part in ZWD (Duan et al. 1996). (Bevis et al. 1994) found that 1 mm of PWV produces a 6.35 mm delay of GNSS signals and can oscillate about 20%, depending on the geographical, the seasonal, and the meteorological conditions.

3. PREDICTION OF TYPHOON PATH BASED ON GNSS-PWV

3.1 Study Site Description

South Korea is located in the mid-latitudes of the Northern Hemisphere (from 33.25 to 38.38° N). On the east coast of the Eurasian Continent and adjacent to the Western Pacific, South Korea has both continental and oceanic climate features. In South Korea, there are 186 GNSS stations, 95 Meteorological Stations (MT station), and 7 Radiosonde stations (RS station) separated by approximately 15, 25, and 178 km on average, respectively as shown in Fig. 1. GNSS stations are much more densely distributed than RS stations, and MT stations are enough to provide the surface temperatures with GNSS stations to convert PWV. Therefore, this study area is the best to investigate the variation of GNSS-PWV elaborately.

Each summer, approximately 30 typhoons are generated in the Northwest Pacific Ocean. Of these, two to three of them broadly impact the local weather system of South Korea, with 20% of these making direct landfall (Korea Meteorological Administration 2010). In this study, we investigated two typhoons—Soulik and Kongrey typhoons, which occurred in August and October in 2018, respectively. These two typhoons were selected for the case study because of their distinctive characteristics. Soulik occurred in August, which is common as many other typhoons. However, its path did not follow the pattern of the regular typhoons in South Korea (i.e., the ones penetrating the central part of South Korea), and there was another typhoon, Cimaron, which occurred nearby during its passage. Besides, many of the weather forecast

agents had difficulty forecasting the typhoon path (Gwonpil Chun 2018, the Herald Corporation 2018, Park et al. 2019).

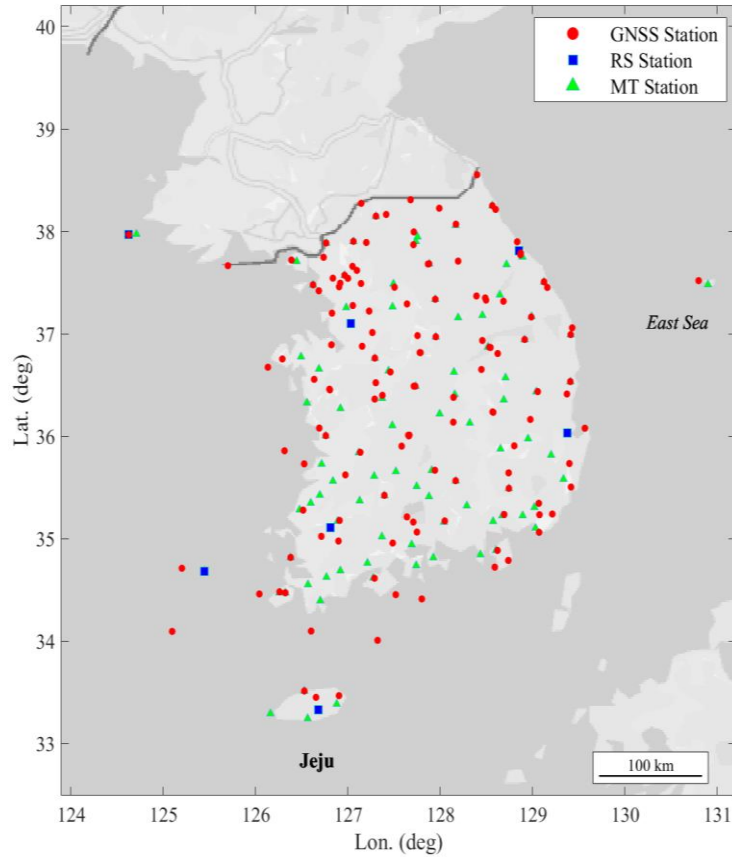


Fig. 1. The distribution of GNSS stations, RS stations and MT stations in South Korea. Jeju is the southernmost island of South Korea, where Soulik and Kongrey both passed.

On the other hand, Kongrey was unusual in that it took place in October, a period much later than the characteristic summer occurrence. Although Kongrey also made landfall as Soulik did, many of the weather forecast agencies managed to forecast its path correctly. In describing the status of each typhoon at specific points in time, we used South Korea's official typhoon classification, as explained in Table 2.

Soulik was the first typhoon, which made landfall since 2012 (National Typhoon Center 2019) as many typhoons tend to pass over the ocean without landfall in the Korea Peninsula. It was formed on August 16 in 2018 at 00:00 (UTC) in the Philippine Sea (15.2 °N, 143.2 °E). After

passing near Japan, early on August 22, the typhoon gradually weakened due to the low sea-surface temperatures. On August 23, the typhoon made landfall over the southwest part of South Korea with a moderate intensity. Since Soulik was about to make landfall, another typhoon, Cimaron, came up near Japan and influenced Soulik. On August 24, at about 01:00, Soulik left South Korea, having been moving 412.65 km for 11 hours inland. Soulik was challenging for most of the forecast agencies in the world as to whether it would make landfall on South Korea or just go through Korean strait as usual, as shown in the official forecasts made by Korea Meteorological Administration (KMA) as shown in Fig. 2. In Fig. 2, the accuracy of ‘-5h forecast’ did not improve than ‘-8h forecast’, rendering Soulik was very challenging to predict. Moreover, KMA was barely able to forecast its path only 1 hour ago. The forecasts for Kongrey, on the other hand, remained accurate and consistent over time.

Kongrey was developed on September 29 in 2018 at 06:00 near Pohnpei island in the Federated States of Micronesia (12.5 °N, 142.7 °E). It made landfall on the study area on October 6 at around midnight, and its intensity was classified as a moderate typhoon. Kongrey went through the southeast part of the study area, 190.2 km long, for 3.7 hours. As shown on the right side of Fig. 2, KMA forecasted its path and the landfall point to a satisfactory level.

Table 2. Typhoon Classification in South Korea

Size¹		Intensity²		
Classification	Range (km)	Classification	Pattern	Maximum sustained wind speed (m/s)
Extra Large	More than 800	Super strong		More than 54
Large	800 – 500	Very strong	Typhoon (TY)	54 – 44
Medium	500 – 300	Strong		44 – 33
Small	Less than 300	Normal	Severe Tropical Storms (STS)	33 – 25
		-	Tropical Storm (TS)	25 – 17

1 The size of the typhoon is divided into stages based on the strong wind radius (the distance from the center of the typhoon to the wind blowing at least 15 m/s).

2 The intensity of a typhoon is classified according to the maximum wind speed of the central region (10 minutes average).

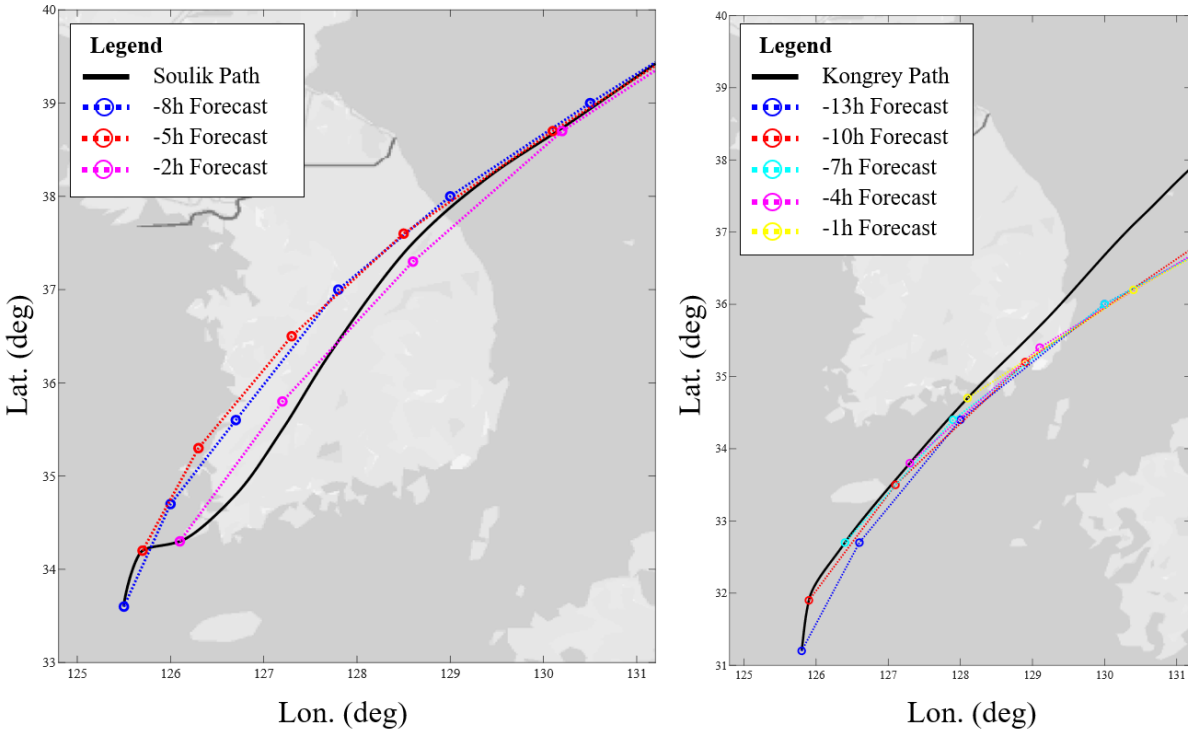


Fig. 2. The forecasted paths of Soulik (left) and Kongrey (right) by KMA. All the circles in both forecasts were made at an interval of 6 hours. The negative time in the legend indicates the hours before a typhoon makes landfall.

3.2 Computation of GNSS-PWV

To extract PWV in the area of interest, the raw GNSS data were acquired from GNSS Integrated Data Center in South Korea (<http://www.gnssdata.or.kr>). It provides GNSS data from the 186 permanent stations, which are run by seven different governmental agencies. Of the 186 stations, we used 135 stations due to the technical issues at 51 stations. Each station records data at 30 seconds intervals, and this study used Global Positioning System (GPS) data of GNSS data. To estimate ZWD, GIPSY-X 1.2 software was used. GIPSY-X is the recent version of GIPSY, which was developed by NASA Jet Propulsion Laboratory (JPL) for the GNSS data processing in Precise Point Positioning (PPP) strategy. GIPSY was the first GNSS software to implement a stochastic estimation approach based on a Square Root Information Filter (SRIF) for atmospheric parameters instead of the deterministic parameter estimation (Bevis et al. 1992) so that GIPSY has been considered as one of the most robust GNSS PPP software estimating ZWD. In this

study, ZWD was modeled as a random walk process (Larson et al. 2001) at an interval of 5 minutes to restrain the observational noise. The positions of the GNSS stations were fixed for mitigating the correlation between the height estimates of the receiver and ZWD estimates (Li et al. 2003). In this study, Global Mapping Function (GMF) was used as a mapping function of ZWD (Böhm et al. 2006); for estimating ZHD, the Saastamoinen model was used (Saastamoinen 1972); for the final products of the satellites, the precise ephemeris provided by JPL were used; and for eq. (4), T_s is obtained from MT stations.

The processed GNSS-PWV was validated with the RS-PWV. Fig. 3 shows the GNSS-PWV and the RS-PWV measured at the stations in Jeju as Jeju is a common point shared by the two typhoon paths. When KMA acquires the upper air data, they send the data to the World Meteorological Organization's Global Telecommunication System (GTS). Then, Wyoming Weather Web (<http://weather.uwyo.edu/upperair/sounding.html>) calculates the RS-PWV based on the data stored GTS (Evans et al. 2012). These RS-PWV data were used for validating the GNSS-PWV in Jeju. The upper plots in Fig. 3 present the GNSS-PWV and RS-PWV in a time domain. The general trends between the two measurements are similar, while a slight offset between two datasets was observed in the Soulik case (left). This offset can be explained by the inconsistent location of the balloon when it collected samples. The lower plots in Fig. 3 shows the correlation between the two datasets. During the two typhoons' cycle, the R-squares of RS-PWV vs. GNSS-PWV are 0.7174 for the Soulik case and 0.8967 for the Kongrey case, respectively. The general trends of the two cases show a good agreement with each other.

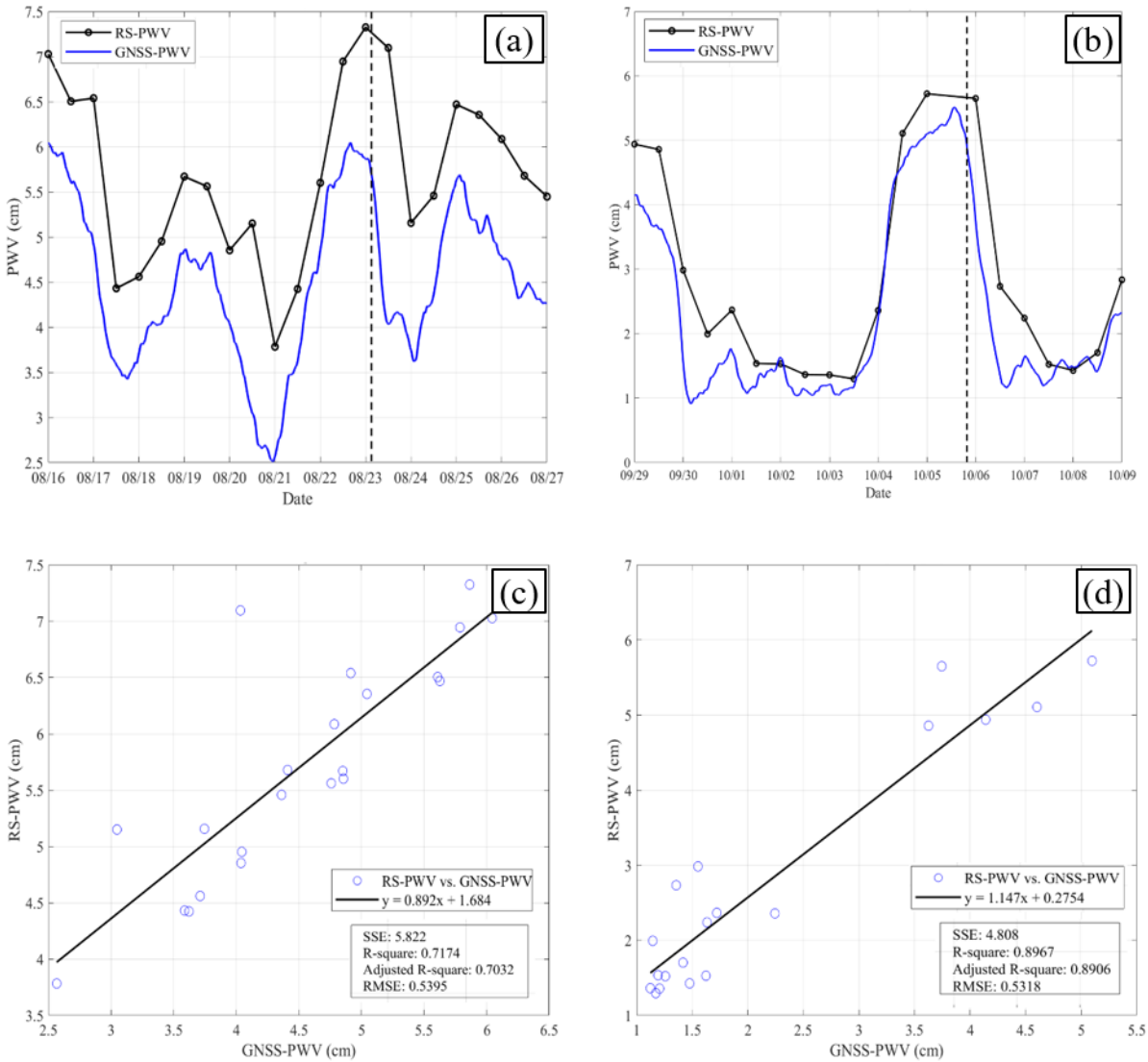


Fig. 3. The comparison between GNSS-PWV and RS-PWV in Jeju, during the whole cycle of each typhoon. The GNSS station (JJBG) and RS station are 13.8 km apart. The dashed vertical lines in (a) and (b) indicate the time that each typhoon approached the GNSS station, 98.15 km for Soulik, and 26.2 km for Kongrey, respectively. (c) and (d) show the relationship between two PWVs, in terms of R-square. It is assumed that the difference between two PWVs is attributed to the typhoon’s characteristics, such as the wind speed, the size of a typhoon, and seasonal factors, such as pressure and temperature variance.

3.3 Prediction Technique Based on PWV

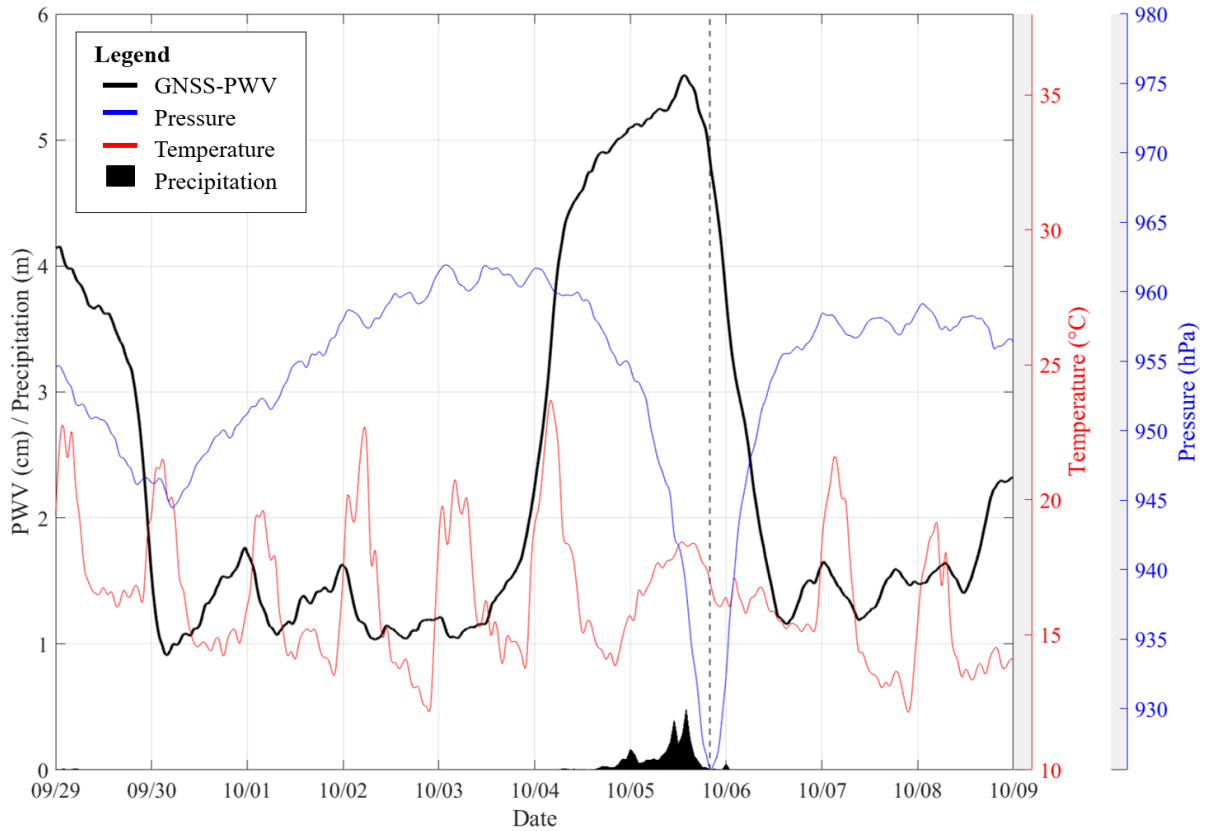


Fig. 4. The time series of PWV, pressure, temperature, and precipitation in Jeju during the whole cycle of Kongrey; Each data was generated at the interval of 5-minute for GNSS-PWV and 1-hour for temperature, pressure, and precipitable. The dotted vertical line is the time Kongrey was the closest to Jeju. Note that the unit of precipitation is meter, whereas the unit of GNSS-PWV is centimeter.

The progress of a typhoon is characterized by a significant change of PWV over a region. In this study, we assume the increased atmospheric water vapor over a region can be an indicator of the typhoon's movement because the variation of regional PWV is highly related to that of the typhoon (Song& Yun 2006). As discussed earlier, GNSS is one of the most suitable tools to capture the variation of the regional PWV in real-time, making the change of tracking in PWV fast and efficiently. Besides, the Korean peninsula contains a dense GNSS network that allows

monitoring real-time changes with high resolution. Therefore, the research model is a favorable option for monitoring the path of a typhoon.

Before looking into the variation of GNSS-PWV, this study investigated the variation of PWV and atmospheric parameters in time series to validate their correlation with the cycle of a typhoon, as shown in Fig. 4. The distance between the GNSS station and the MT station used in Fig. 4 was 13.57 km, and the closest distance between the typhoon and the GNSS was 26.24 km, respectively. Since a typhoon brings much rainfall, the relationship between GNSS-PWV and precipitable must be highly correlated. Studies have attempted to prove this relationship (Manandhar et al. 2016, Yao et al. 2017, Zhao et al. 2018), but high PWV does not always guarantee the precipitation due to the complexity of precipitation causes (Seco et al. 2012, Shoji 2013). In some cases, low water vapor in the atmosphere brings precipitation or high water vapor does not accompany precipitation.

In most cases, the pressure is a crucial factor in predicting a typhoon path. When a typhoon approaches, the pressure starts to decrease (National Typhoon Center 2011), and the typhoon typically moves to the direction of the pressure trough. When Kongrey had the shortest distance with the MT stations, the pressure was the lowest as expected, which was shown in Fig. 4. In the meantime, the trend of GNSS-PWV showed the opposite tendency where it reached the peak slightly earlier than the trough of the pressure. This contrary trend was found in most of the other stations, and it implies that GNSS-PWV also can be used for predicting the typhoon path.

Temperature is another important meteorological element. When PWV remained high during the approach of the typhoon, the range of temperature was relatively low. During the period of the typhoon, the average daily temperature remained lower than other days because the correlation between precipitation and temperature are negatively correlated during summer. From the observed patterns in Fig. 4, the GNSS-PWV and the meteorological parameters reacted to the coming typhoon, but no significant variations in temperature and precipitation were detected from the selected cases. On the other hand, pressure showed a clear negative correlation to the GNSS-PWV. Consequently, this study focused on only the GNSS-PWV, which also accompanies the pressure variations, to predict a typhoon path.

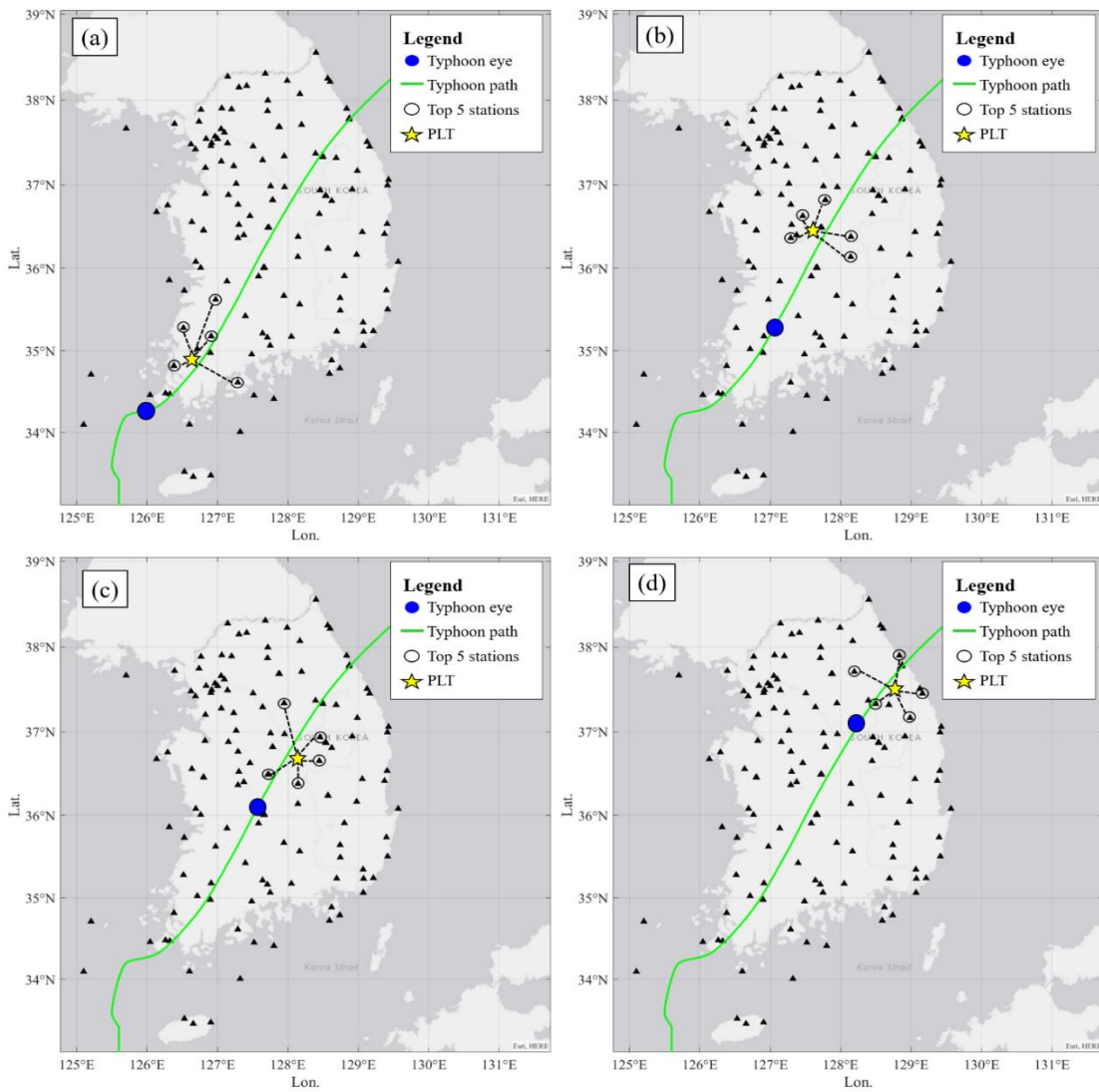


Fig. 5. Determination of PLT based on GNSS-PWV; PTL is calculated at an interval of 5-minute, and (a), (b), (c), and (d) shows the updated typhoon location and the corresponding PLT, sequentially.

For the prediction of the typhoon path, the variations of PWV caused by the typhoon's progress were monitored with GNSS in the study area, at an interval of 5-minute for the whole cycle of the typhoon. As the PWV is considered as the indicator of the movement of a typhoon, the GNSS stations having the high PWV reading were selected for predicting the expected locations of typhoons. The selected stations were considered as a cluster for determining the Predicted

Location of Typhoon (PLT) at each recorded epoch. The PLT in this study is based on the two-dimension location of the selected stations—the latitude and the longitude like other conventional typhoon forecasts (National Typhoon Center 2019, Joint Typhoon Warning Center 2020). Fig. 5 demonstrates a few examples for estimating the PLT.

The number of stations in a cluster was empirically determined based on the PWV measurements in the test site. Fig. 6 indicates the PWV measurements from all stations and sorted by the amplitude of PWV. As shown in Fig. 6, the top five stations show distinctively higher PWV values apart from other stations. From the selected cluster, the center point of the cluster was considered as the PLT, which is the yellow star in Fig. 5. described in Table 3, the mean of PLTs is distinctively higher than that of the rest stations. Moreover, the mean of PLT increased from t1 to t2 as the typhoon approached the study area, GNSS stations captured the inflow of PWV into the study area (the time epochs p1 to p4 are addressed in the later section).

Table 3. The statistical comparison, PLT versus the rest stations

		PWV (cm), at t1		PWV (cm), at t2	
		Mean	STD	Mean	STD
Soulik	PLT	6.235	0.285	6.621	0.093
	The rest stations	4.988	0.511	5.662	0.406
Kongrey	PLT	5.599	0.210	5.789	0.198
	The rest stations	4.801	0.453	4.856	0.468

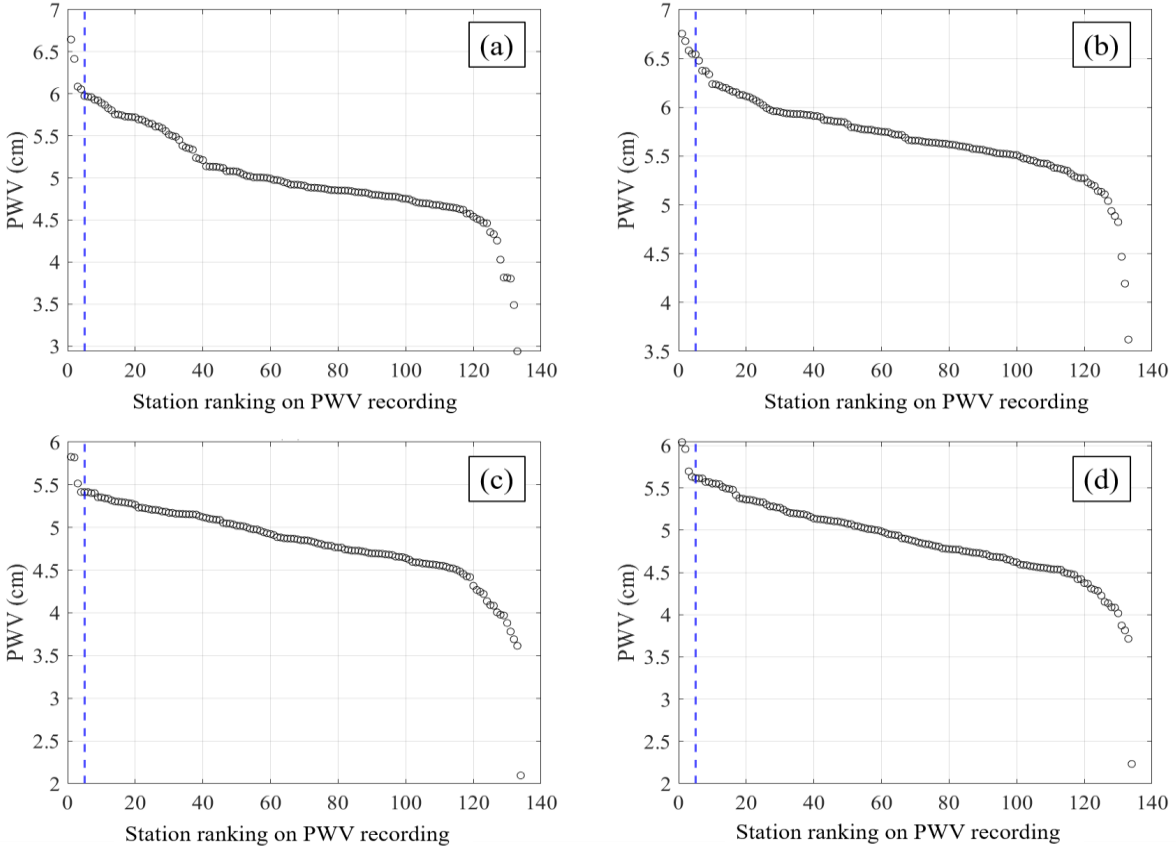


Fig. 6. The scatter plots depict the recordings of PWVs for individual stations sorted in descending order. (a) and (b) represent the distributions of PWV at t1 and t2 for the Soulik case, respectively. (c) and (d) represent the distributions of PWV at t1, t2, and for the Kongrey case, respectively. The stations on the left from the blue dashed line are the top five PWV stations.

It should be noted the PLT is computed based on the locations of the stations after excluding the stations lying outsider of 3 sigma from the center of the cluster, which is a common way of excluding outliers (Wolf& Ghilani 2002).

While calculating PLT, this study also computed the location uncertainty of PLT at each epoch. First, the standard deviations of the longitude and latitude of PLT were calculated, excluding the outliers. Then the propagated uncertainty of PLT was calculated:

$$U = \pm\sqrt{STD_{lon} + STD_{lat}} \quad (6)$$

where U represents the location uncertainty of PLT, STD_{lon} and STD_{lat} is the standard deviation of the longitude and the latitude of PLT, respectively. And a mean of the uncertainties was used for representing the uncertainty of PLT during a typhoon case.

This study, in particular, explored both the timing and accuracy of GNSS-based typhoon pathway prediction by using the PLT. We divide the experimental prediction into three distinct phases with four points according to the behaviors of PLT based on the time epochs of t_1 to t_4 for the actual typhoon's locations. At t_1 , the PLT starts to appear correlated with the coming typhoon; that is, before t_1 , the PLT does not provide any meaningful patterns. This is because the typhoon was located further than the location of t_1 , which does not affect the GNSS stations in the test site so that there is no correlation between the PLT and the typhoon. At t_2 , the PLT starts to show the typhoon's subsequent point. During the period from t_1 to t_2 , which is Phase I, the highest increases of the water vapor in the typhoon are observed only at GNSS stations located along the southern coast because the typhoon is still far away. After t_2 , however, the typhoon is close enough for the inland GNSS stations to capture the inflow of water vapor so that the PLT can show the predicted typhoon location. t_3 is when the PLT is disturbed or restricted because of exogenous factors, such as the influence of another typhoon, or due to the fact that GNSS stations are not established in the ocean. Phase II is, therefore, the time period between t_2 and t_3 that is the most applicable for the proposed study considering the spatial distribution of GNSS stations. t_4 is when the typhoon leaves South Korea inland. Phase III is defined for the time period between t_3 and t_4 .

Phase I: PLT converges toward a point on the pathway (between t_1 and t_2)

Phase II: PLT begins to generate the predicted typhoon path (between t_2 and t_3)

Phase III: PLT is hindered (between t_3 and t_4)

The p_1 to p_4 indicates locations of PLTs at the epochs from t_1 to t_4 .

4. EXPERIMENT RESULTS AND VALIDATION

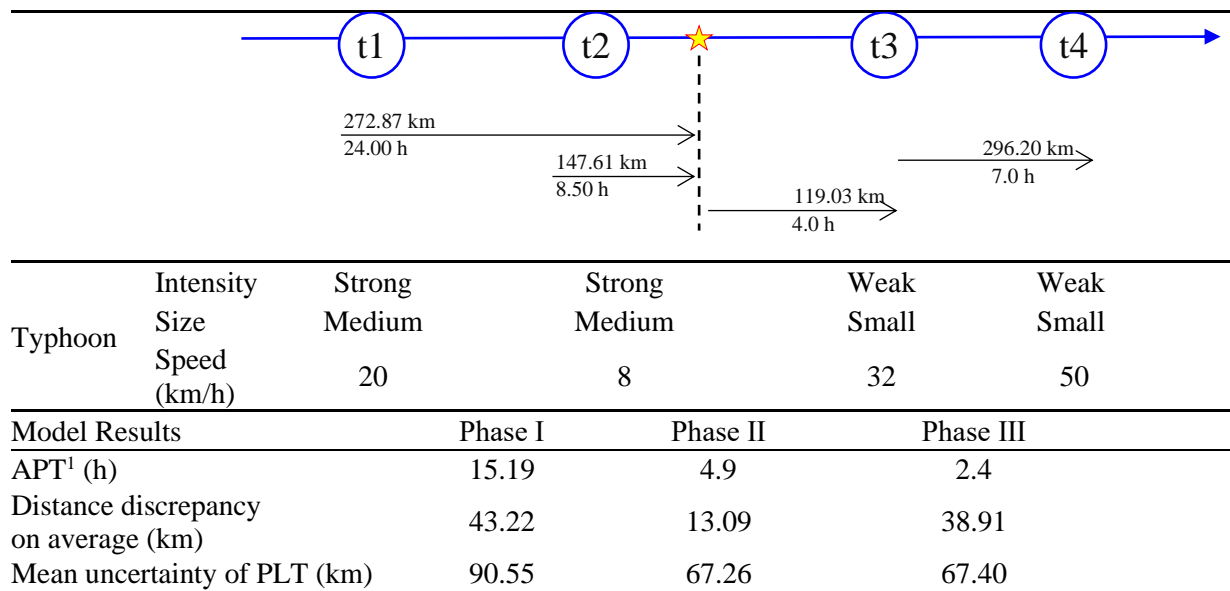
This section presents the results of the predicted path for two typhoon events by the determined PLT using GNSS-PWV, as described in Section 3. The two typhoons, Soulik and Kongrey, were

severe events that directly impacted the Korean peninsula, enabling the use of the terrestrial GNSS stations to predict the expected storm pathways. Thus, this section assesses related questions that are 1) how early in advance can the PLT predict a subsequent typhoon’s location? And 2) what level of the distance discrepancy (in km) would the PLT have? As addressed before, to answer those two questions, the PLT was used to predict the landfall point and the subsequent point on the typhoon’s path.

4.1 Soulik

Before t1, where it was 272.9 km, and 24.0 hours before Soulik made landfall, the PLT for Soulik did not show a meaningful pattern until the time epoch of t1, that is p1 for the PLT. As time passed, however, when the typhoon approached t1, the PLT started to converge from p1 to p2, which was Phase I. During Phase I, the research model did not provide a meaningful result because the typhoon was too far to influence inland stations. Fig. 7 shows the resulting path of the PLT and the location tags of the two typhoons—t1 to t4—are marked according to the points p1 to p4. Table 4 explains the Soulik status, and at the same time, the results of the research model, and the PLT, numerically.

Table 4. Soulik status and the results of the research model.



¹ Average Predicting Time (APT) presents how early PLT can predict the location of the typhoon for each phase on average

It should be noted that Phase I in Table 4 (from t1 to t2) showed a large discrepancy between the predicted location and the actual path of the typhoon. As mentioned earlier, this is because of the geographic distribution of GNSS stations that the typhoon did not directly affect the inland stations before its landfall.

Since p2, the PLT became a feasible indicator for predicting the path until p3 that is Phase II, where Soulik moved from t2 to t3, correspondingly. During Phase II, the research model predicted the subsequent locations of Soulik 4.5 hours in advance with an average distance discrepancy of 13.1 km and a mean of the uncertainties of 67.26 km, as shown in Table 4; i.e., after the typhoon location of t2, the PWV of Soulik inflowed into the study area, and these increases were captured at inland GNSS stations. Due to the simultaneity between the movements of PWV and the typhoon, the approach of PWV was described as the predicted typhoon location with PLT. In a real-time and local prediction perspective, this result can be used in a short-term prediction with a local scale.

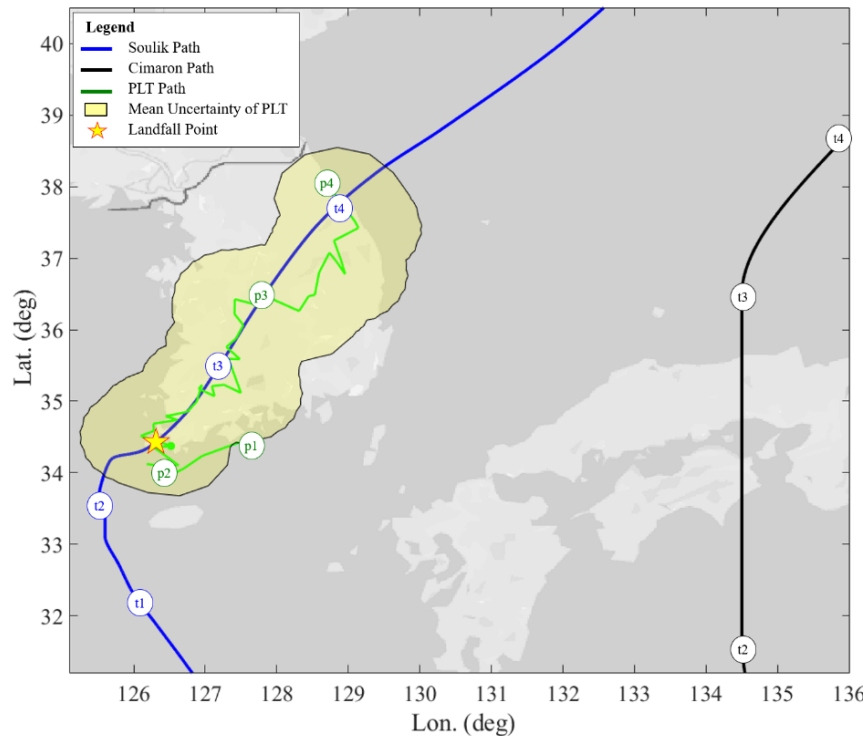


Fig. 7. The result of the research model during the Soulik event. When Soulik was moving from t1 to t2, PLT was also moving from p1 to p2 (Phase I), corresponding to the movement of Soulik.

As far as the landfall point is concerned, the predicted landfall point made by the PLT was the location where the PLT first met the inland study area during Phase II. The PLT predicted the landfall point 6 hours before with an average distance discrepancy of 19.1 km, which was 2.5 hours after p2. This result is noteworthy, compared to the official forecasts in Fig. 2, where KMA forecasted the landfall point 5 hours before with an average distance discrepancy of 123.1 km, as addressed in Table 8. This large discrepancy in the official forecast was led by Cimaron, which started to draw Soulik in the eastern direction and delay the process of Soulik at around t2 (National Typhoon Center 2019). On the other hand, the PLT was able to reflect the movements of PWV in Soulik so that it was able to point out to the landfall point, more accurately.

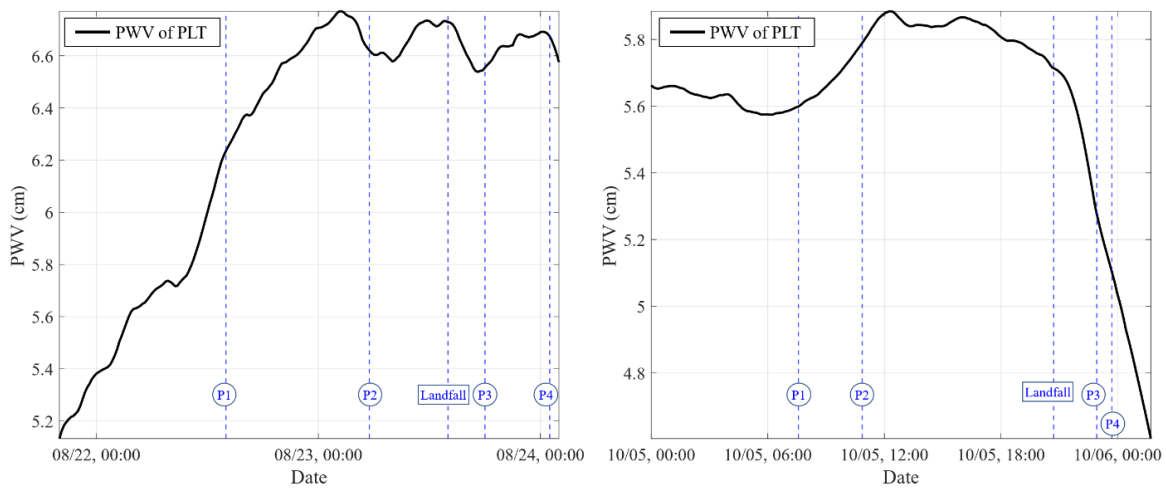


Fig. 8. The recordings of the PWV of the PLT—the left for Soulik and the right for Kongrey. The blue dotted lines are at specific points where the Phases are divided, or the typhoon made landfall.

As shown in the left panel of Fig. 8, the PWV of the PLT decreased about two hours before p2. According to the 2018 Analysis Reports of Typhoon, the intensity of Soulik was weakened around the time of p2 due to the upwelling in Jeju sea (National Typhoon Center 2019). The PWV of the PLT increased again a few hours after p2, the cause of which came from the inflow of PWV from Cimaron. Then, after landfall, the PWV decreased again due to the ground friction between the typhoon and the ground.

During Phase II, Cimaron delayed the movements of Soulik and influenced the GNSS-PWV of the Soulik case. As the typhoon Soulik had advanced to t3, Soulik and Cimaron had the shortest distance of 666 km. It is thought that by that time, the influence of Cimaron on Soulik was the greatest. Consequently, PLT at around p3 was disturbed, as shown in Fig. 7. Specifically, the left panel of Fig. 8. depicts the PWV of the PLT in the Soulik case that the PWV again increased at p3 when Cimaron approached Soulik the nearest. Based on the two abnormal increases of PLT of PWV, it is indicated that PLT captured the inflow of water vapor of Cimaron. Hence, it is another excellent example of how sensitively GNSS meteorology can capture the variation of water vapor.

Table 5. The result of the research model for the Soulik case.

	Prediction made at	Actual passage at	Prediction time (hours) ¹	Distance discrepancy (km) ²	Uncertainty of PLT (km)
p1	08-22, 14:00	08-23, 15:50	25.8	113.2	126.01
	08-22, 18:00	08-23, 12:27	18.5	54.4	90.81
	08-23, 02:00	08-23, 12:29	10.5	30.8	91.17
p2	08-23, 05:30	08-23, 13:33	8.1	19.9	57.93
	08-23, 09:00	08-23, 15:57	7.0	1.8	39.37
	08-23, 14:00	08-23, 17:28	3.5	51.3	33.33
p3	08-23, 18:00	08-23, 21:30	3.5	2.0	110.95
	08-23, 21:00	08-23, 23:31	2.5	64.0	97.66
p4	08-24, 01:00	08-24, 01:10	0.2	27.3	29.08

1 Prediction time means ‘Actual passage at – Prediction made at.’ i.e., it shows how early in advance PLT

2 Distance discrepancy means between the actual typhoon location and the predicted location. i.e., it shows what level of the distance error PLT had.

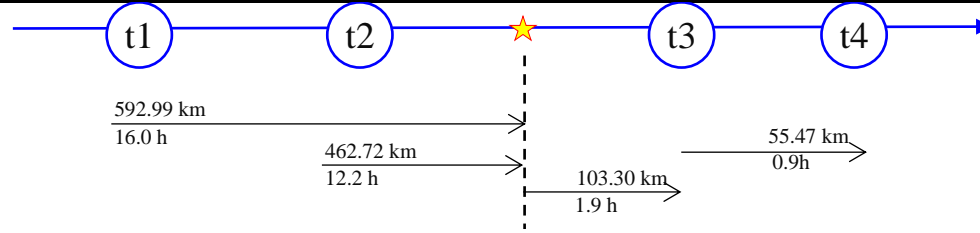
After Soulik was intervened by Cimaron, it continued to move northeastward 296.2 km until the typhoon departed South Korea—Phase III. Its statistical values were shown the location with 2.4 hours in advance, with an average distance discrepancy of 38.9 km and with a mean of the uncertainties of 67.40 km, despite the effect of Cimaron. The overall prediction results are addressed in Table 5. To evaluate the performance of the research model, several epochs in each phase were selected and compared the predicted PLT and the actual path. The first column indicates the selected time epochs, and the second column presents the time that the typhoon passed the closest to the determined PLT at each epoch. By comparing these two columns, one can find how much in advance the prediction was made for the passage of typhoon, which is the

third column. The fourth column in Table 5 is the distance between the PLT and the actual location of typhoon at each epoch. The last column, the uncertainty of PLT, indicates the precision of the PLT from the cluster of top five PWV stations, which is U in eq. (6).

4.2 Kongrey

Before t_1 , where it was about 593.0 km and 16 hours earlier than the Kongrey landfall, the PLT for the Kongrey case did not yet show any discernible patterns until the time epoch of p_1 . When the typhoon moved from t_1 to t_2 , however, the PLT started correspondingly to converge from p_1 to p_2 —Phase I. Fig. 9 shows the resulting path of the PLT and the location tags of the typhoon (t_1 to t_4) are marked corresponding to the point, p_1 to p_4 . Table 6 explains the Kongrey status, and at the same time, the results of the research model by PLT, numerically.

Table 6. Kongrey Status and the results of the model



Typhoon	Intensity	Moderate	Moderate	Moderate	Moderate
	Size	Medium	Medium	Small	Small
	Speed (km/h)	30	37	53	55
Model Results		Phase I	Phase II	Phase III	
APT (h)		10.28	4.05	0.48	
Distance discrepancy on average (km)		54.18	19.01	20.88	
Mean uncertainty of PLT (km)		88.82	73.75	138.15	

After Phase I, the PLT generated the predicted typhoon location until the PLT met the easternmost part of the predicted path, p_3 —Phase II. During Phase II, Kongrey was traveling 570.0 km for 14.1 hours, from t_2 to t_3 . After p_3 , the PLT method cannot be applied farther due to the geographic limitation regarding the available GNSS stations' location. In Phase II, the PLT managed to predict the typhoon's subsequent locations, 4.1 hours early, with an average distance discrepancy of 19.0 km and with a mean of uncertainties of 73.75 km, as addressed in Table 8.

Concerning the landfall point, the official forecasts had an average distance discrepancy of 40.5 km for the five forecasts in Fig. 2, which could be considered as an acceptable forecast result compared to the case of Soulik. On the other hand, the PLT predicted the landfall point 4.7 hours earlier with a distance discrepancy of 7.3 km than the actual landfall, in Table 8. The predicted landfall point also was the first place where the PLT met on the study area after p2, similar to the Soulik case. In terms of uncertainty, the research method was compelling in a short-term prediction and a local scale.

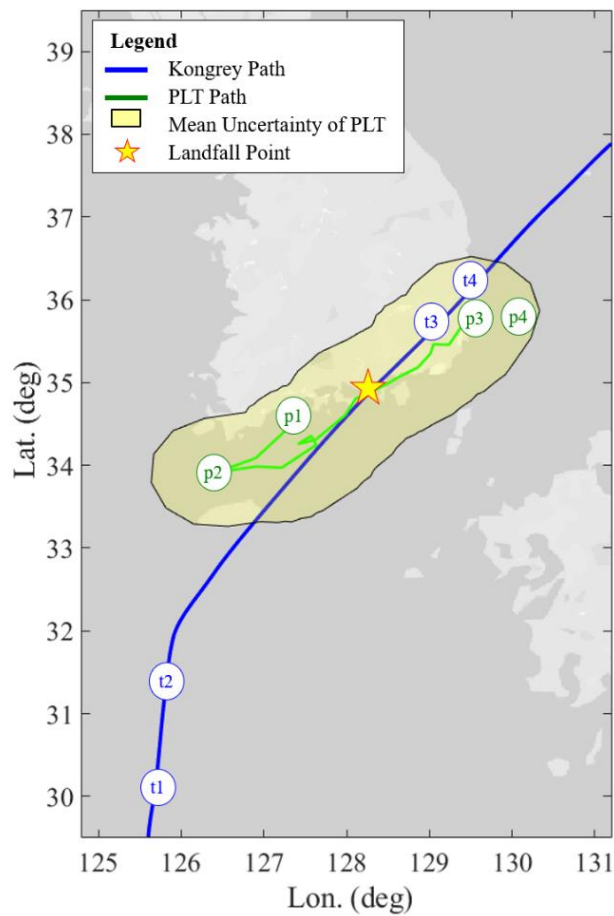


Fig. 9. The result of the research model during Kongrey

During Phase III, Kongrey moved 55.5 km for 55 minutes and left southeastern South Korea. The research method predicted the subsequent locations of Kongrey 0.5 hours in advance with an average distance discrepancy of 20.9 km, in Table 6. As pointed earlier, the PLT approach is not feasible during this phase because the typhoon stays near the edge of inland so that the further

stations along the path do not exist. The overall results of the method are shown in Table 7. The interpolation of Table 7 is the same as Table 5, as in Section 4.1. The overall comparison between the official forecast and the research model was addressed in Table 8.

Table 7. The result of the proposed model for the Kongrey case.

	Prediction made at	Actual Passage at	Time discrepancy (hours)	Distance discrepancy (km)	Uncertainty of PLT (km)
p1	10-05, 08:45	10-05, 22:35	13.83	22.16	163.45
	10-05, 10:45	10-05, 20:54	10.15	54.43	85.36
	10-05, 11:45	10-05, 20:54	9.15	54.43	85.36
p2	10-05, 12:40	10-05, 20:00	7.33	82.27	90.81
	10-05, 19:30	10-06, 00:10	4.67	7.28	56.90
	10-05, 23:30	10-06, 02:12	2.70	20.55	78.62
p3	10-06, 02:45	10-06, 03:26	0.68	20.88	138.15
	10-06, 03:20	10-06, 03:26	0.10	20.88	138.15
p4	10-06, 03:40	10-06, 03:26	0.77	20.88	138.15

4.3 Comparison

At p1, the PLT reacted 8 hours earlier in the Soulik case than in the Kongrey case, but 320.1 km closer to the landfall point in the Soulik case. At p2, however, the PLT showed the typhoon’s subsequent location earlier and farther in the Kongrey case than in the case of Soulik, as compared Table 4 and Table 6. Although there was no difference in terms of the sizes of the two typhoons, which is recorded as “medium,” the movements of PLT was distinctive where the inflow of the water vapor was captured earlier in the Kongrey case that can be interpreted as the span of the water vapor in the Kongrey case was more extensive than in the Soulik case.

During Phase II, the PLT functioned 12.5 hours, 266.6 km in the Soulik case, and 14.1 hours and 570.0 km in the Kongrey case, respectively. The difference in the distance came from the speed of each typhoon—Kongrey was faster than Soulik. The results of the PLT shows 4.5 APT with an average distance discrepancy of 13.1 km for the Soulik case and 4.1 APT and 19.0 km for the Kongrey case, respectively. Although PLTs in both cases couldn’t work for the different reason—in the case of Soulik, the PLT was disturbed by Cimaron from around t2, whereas in the

Kongrey case, the PLT was not applicable due to the spatial limitation—in general, their results seem similar and consistent, which means PLT yields reliable and acceptable results.

Table 8. The comparison of the research model and the official forecast in each case.

		Landfall Prediction			Phase II	
		KMA		PLT	KMA	PLT
Soulik	ATP (h)	8.0	5.0	6.0	(-5 hours) ¹	4.9
	Discrepancy (km)	70.19	123.07	19.09	70.86 (144.08) ²	13.09 (67.26) ³
Kongrey	ATP (h)	7.0	4.0	4.7	(-7 hours)	4.1
	Discrepancy (km)	40.82	40.17	7.28	50.57 (94.03)	19.01 (73.75)

1 forecasting hours before landfall.

2 the maximum discrepancies in distance

3 The average uncertainty of PLT throughout the path in Phase II

As shown in Table 8, the mean uncertainty of PLT during Phase II is 67.26 km and 73.75 km for the cases of Soulik and Kongrey, respectively, which are reasonably consistent. The average distance discrepancies of two cases also are consistent that are 13.09 km and 19.01 km for Soulik Kongrey, respectively.

For the prediction of the landfall point, the official forecasts in the Soulik case produced inaccurate results over time, as shown in Fig. 2. In the Kongrey case, however, the official forecasts from KMA stayed consistent and functioning well. Comparing the research results to the official forecasts in Fig. 10, the proposed research model followed the overall trace of the actual movement of both typhoons. In the case of Soulik, the proposed model was closer to the ground truth except for the time period of the Cimaron effect. In the Kongrey case, the proposed model showed closer to the actual path than the result from KMA. Table 8 organizes the comparisons, as mentioned earlier.

It should be noted that the PLT was determined based on a particular epoch of user input and provide the predicted location without specifying the time information because this method did not consider the prediction in the time domain while the official forecast by KMA forecasts the path of typhoon with an interval of 6 hours.

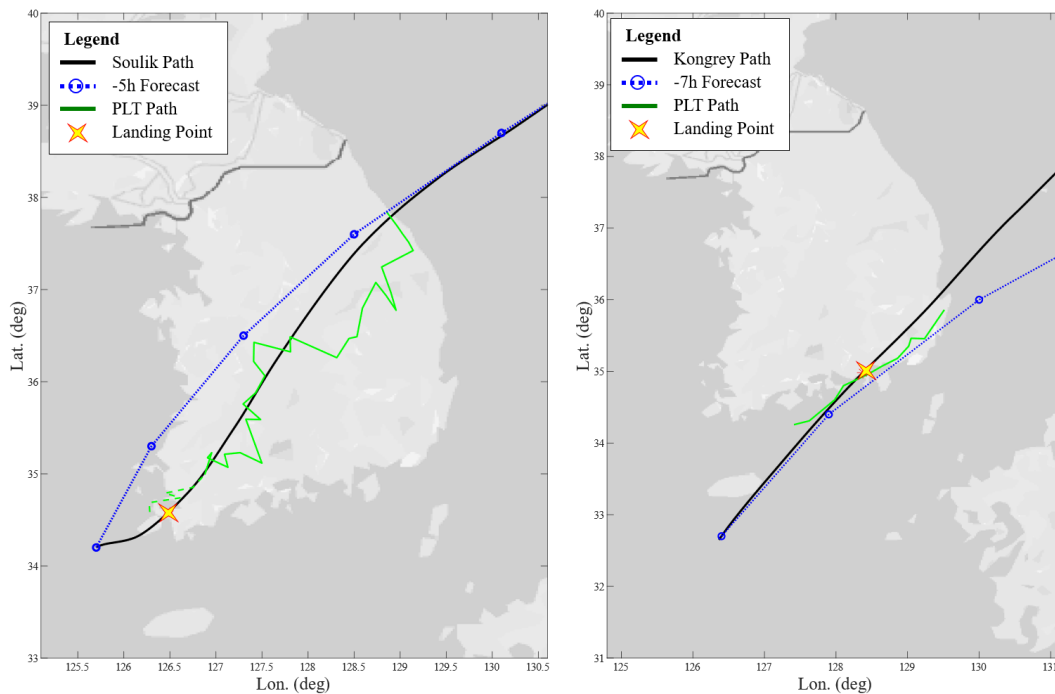


Fig. 10. Comparison of the forecasts, the left for Soulik and the right for Kongrey. PLT path—solid green lines—start when each typhoon and the forecasts start. For the Soulik case, the green dotted line means the previous PLT path from the typhoon landfall to the -5h forecast made

5. SUMMARY AND CONCLUSION

The frequency, intensity, and duration of tropical cyclones have increased since the early 1980s, which also increase socioeconomic losses (Jet Propulsion Laboratory 2020). To minimize the impact of weather hazards, including typhoons and hurricanes, a proper forecast is crucial. This study specially focused on predicting the landfall point and the path of typhoons by observing the variations of GNSS-PWV. Also, in many countries, GNSS stations are densely distributed, which makes it possible that the PLT works there, providing better spatiotemporal resolution than the radiosonde. Finally, based on the case studies, the research method yielded consistent and satisfactory, despite the different characteristics.

In this study, primary meteorological parameters were analyzed and found the impact of typhoons in pressure and PWV. Also, the inflow of water vapor influenced temperature and precipitation, although those two parameters did not show the information on the typhoon's path.

Another finding was the pattern of air pressure, which was negatively correlated to GNSS-PWV. Therefore, this study focused on the GNSS-PWV only, rather than combining multiple parameters for the prediction model.

Given the assumption that the variation of regional PWV could be an indicator of the typhoon's movement, we proposed the research model using PLT. To compute the PLT, the top five GNSS stations showing the highest PWV were selected, and their mean location showed the subsequent point on the typhoon's path. The PLT was tested to answer the two questions: how early in advance the PLT can predict a typhoon's subsequent location, and what level of the distance discrepancy (in kilometers) the prediction would have. Our analysis showed that the PLT could predict a typhoon's subsequent locations, approximately 4 hours earlier, with an average distance discrepancy of approximately 19 km in both cases. Moreover, in the Soulik case, the PLT was able to capture the two abnormal increases of GNSS-PWV, which was caused by the adjacent typhoon, Cimaron. Meanwhile, the PLT could predict landfall points 6.0 hours earlier with a distance discrepancy of 19.1 km for the Soulik case, and 4.7 hours earlier with a distance discrepancy of 7.3 km for the Kongrey case, respectively. Based on the two results, the research method can be reference information for a short-term prediction of the landfall point with high accuracy.

The proposed model utilized only one parameter, GNSS-PWV, and was designed with a straightforward algorithm, taking advantage of pre-existing GNSS stations. While conventional meteorology requires that new radiosondes be launched for each study, GNSS meteorology does not similarly require extra measures. Moreover, the research model could work in the severe weather conditions seamlessly in a cost-effective and eco-friendly fashion. Although we selected typhoons as the case study, the proposed method is applicable to hurricanes, which is another class of tropical cyclones.

For future research, it is worth considering the effects of GNSS station's altitude on the movements of regional PWV—in general, the higher the altitude of the station, the lower the PWV. Accordingly, if we can normalize GNSS-PWV considering the altitude of the station, the PWV can better reflect the movement of the PWV. Another possibility for refining predictions can be explored by implementing filters, such as the Kalman filter. When such a filter is applied,

the path of a typhoon appears smoother, and thus it can provide a more accurate picture of the typhoon's trajectory. As regards the current forecast manner, it can provide typhoon forecasts in a few days, but sometimes their uncertainties in time and distance are not negligible. The research method, in contrast, can provide reliable and consistent results in time and distance, but it provides only the subsequent location of a typhoon in a few hours. Thus, this research will be supplementary for the current severe weather forecast methods.

BIBLIOGRAPHY

Askne, J. and H. Nordius (1987). "Estimation of tropospheric delay for microwaves from surface weather data." Radio Science **22**(03): 379-386.

Bevis, M.S. BusingerS. ChiswellT. A. HerringR. A. Anthes et al. (1994). "GPS meteorology: Mapping zenith wet delays onto precipitable water." Journal of applied meteorology **33**(3): 379-386.

Bevis, M.S. BusingerT. A. HerringC. RockenR. A. Anthes et al. (1992). "GPS meteorology: Remote sensing of atmospheric water vapor using the Global Positioning System." Journal of Geophysical Research: Atmospheres **97**(D14): 15787-15801.

Böhm, J., A. Niell, P. Tregoning and H. Schuh (2006). "Global Mapping Function (GMF): A new empirical mapping function based on numerical weather model data." Geophysical Research Letters **33**(7).

Bordi, I., T. Razinei, L. S. Pereira and A. Sutera (2014). "Ground-Based GPS Measurements of Precipitable Water Vapor and Their Usefulness for Hydrological Applications." Water Resources Management **29**(2): 471-486.

Davis, J., T. Herring, I. Shapiro, A. Rogers and G. Elgered (1985). "Geodesy by radio interferometry: Effects of atmospheric modeling errors on estimates of baseline length." Radio science **20**(6): 1593-1607.

Duan, J.M. BevisP. FangY. BockS. Chiswell et al. (1996). "GPS meteorology: Direct estimation of the absolute value of precipitable water." Journal of applied meteorology **35**(6): 830-838.

Elliott, W. P. and D. J. Gaffen (1991). "On the utility of radiosonde humidity archives for climate studies." Bulletin of the American Meteorological Society **72**(10): 1507-1520.

Evans, M., J. Constantino, B. Lambert and R. Grumm (2012). "A PRELIMINARY STUDY OF INVERTED-V SOUNDINGS AND DOWNSTREAM SEVERE WEATHER IN NEW YORK AND PENNSYLVANIA." National Weather Digest **36**(1).

Gutman, S. I. and S. G. Benjamin (2001). "The role of ground-based GPS meteorological observations in numerical weather prediction." GPS solutions **4**(4): 16-24.

Gwonpil Chun (2018). The path of Typhoon Soulik, Korea Meteorological Administration (KMA) is on and off. the Joonganilbo. South Korea, the Joonganilbo.

Hofmann-Wellenhof, B., H. Lichtenegger and E. Wasle (2007). GNSS—global navigation satellite systems: GPS, GLONASS, Galileo, and more, Springer Science & Business Media.

Hogg, D., F. Guiraud and M. Decker (1981). "Measurement of excess radio transmission length on earth-space paths." Astronomy and Astrophysics **95**: 304-307.

- Jet Propulsion Laboratory. (2020, 07/07/2020). "The effect of Climate Change." Retrieved 07/11/2020, 2020, from <https://climate.nasa.gov/effects/>.
- Joint Typhoon Warning Center. (2020, 10.01.2018). "Best Track Archive." Retrieved 04.23, 2020, from <https://www.metoc.navy.mil/jtwc/jtwc.html?best-tracks>.
- Kanda, M. (2000). "Analysis of temporal and spatial change of a convective thunder storm in Tokyo metropolitan using GPS precipitable water: Case study on 23rd August in 1997." *Tenki* **47**: 7-15.
- Korea Meteorological Administration. (2010). "Climate of Korea." Retrieved 12 April, 2020, from http://www.kma.go.kr/eng/biz/climate_01.jsp.
- Larson, K. M.P. CervelliM. LisowskiA. MikliusP. Segall et al. (2001). "Volcano monitoring using the Global Positioning System: filtering strategies." *Journal of Geophysical Research: Solid Earth* **106**(B9): 19453-19464.
- Li, Z., J. P. Muller and P. Cross (2003). "Comparison of precipitable water vapor derived from radiosonde, GPS, and Moderate-Resolution Imaging Spectroradiometer measurements." *Journal of Geophysical Research: Atmospheres* **108**(D20).
- Lu, J.T. FengJ. LiZ. CaiX. Xu et al. (2019). "Impact of assimilating Himawari-8-derived layered precipitable water with varying cumulus and microphysics parameterization schemes on the simulation of Typhoon Hato." *Journal of Geophysical Research: Atmospheres* **124**(6): 3050-3071.
- Manandhar, S., Y. H. Lee and S. Dev (2016). GPS derived PWV for rainfall monitoring. 2016 IEEE International Geoscience and Remote Sensing Symposium (IGARSS), IEEE.
- National Hurricane Center. (2020). "What is the difference between a hurricane and a typhoon?" Retrieved 07/11/2020, 2020, from <https://www.nhc.noaa.gov/climo/>.
- National Typhoon Center (2011). "Typhoon White Book."
- National Typhoon Center (2019). 2018 Analysis Reports of Typhoon, Korea Meteorological Administration.
- Park, J. H.D. E. YeoK. LeeH. LeeS. W. Lee et al. (2019). "Rapid decay of slowly moving Typhoon Soulik (2018) due to interactions with the strongly stratified northern East China Sea." *Geophysical Research Letters* **46**(24): 14595-14603.
- Saastamoinen, J. (1972). "Atmospheric correction for the troposphere and stratosphere in radio ranging satellites." *The use of artificial satellites for geodesy* **15**: 247-251.
- Seco, A.F. RamírezE. SernaE. PrietoR. García et al. (2012). "Rain pattern analysis and forecast model based on GPS estimated atmospheric water vapor content." *Atmospheric environment* **49**: 85-93.
- Seeber, G. (2008). Satellite geodesy: foundations, methods, and applications, Walter de gruyter.

Shoji, Y. (2013). "Retrieval of water vapor inhomogeneity using the Japanese nationwide GPS array and its potential for prediction of convective precipitation." Journal of the Meteorological Society of Japan. Ser. II **91**(1): 43-62.

Shoji, Y., M. Kunii and K. Saito (2011). "Mesoscale data assimilation of Myanmar cyclone Nargis Part II: Assimilation of GPS-derived precipitable water vapor." Journal of the Meteorological Society of Japan. Ser. II **89**(1): 67-88.

Shoji, Y.H. Nakamura T. Iwabuchi K. Aonashi H. Seko et al. (2004). "Tsukuba GPS dense net campaign observation: Improvement in GPS analysis of slant path delay by stacking one-way postfit phase residuals." Journal of the Meteorological Society of Japan. Ser. II **82**(1B): 301-314.

Soden, B. J., D. D. Turner, B. M. Lesht and L. M. Miloshevich (2004). "An analysis of satellite, radiosonde, and lidar observations of upper tropospheric water vapor from the Atmospheric Radiation Measurement Program." Journal of Geophysical Research: Atmospheres **109**(D4): n/a-n/a.

Song, D. S. and H. S. Yun (2006). "Analysis of GPS precipitable water vapor variation during the influence of a Typhoon EWINIAR." Journal of the Korean Society of Civil Engineers **26**(6D): 1033-1041.

the Herald Corporation (2018). The Korea Meteorological Administration, which is now a "stationary"...Complaints of "rapid weather changes". the Herald Corporation. 08.31.2018.

Wang, J. and L. Zhang (2008). "Systematic errors in global radiosonde precipitable water data from comparisons with ground-based GPS measurements." Journal of Climate **21**(10): 2218-2238.

Weng, F., Y. Ma, H. Yang and X. Zou (2016). Potential Applications of small Satellite microwave observations for monitoring and predicting hurricanes and typhoons. 2016 IEEE International Geoscience and Remote Sensing Symposium (IGARSS), IEEE.

Wolf, P. R. and C. D. Ghilani (2002). Elementary surveying: An introduction to geomatics, Prentice Hall New Jersey.

Yao, Y., L. Shan and Q. Zhao (2017). "Establishing a method of short-term rainfall forecasting based on GNSS-derived PWV and its application." Sci Rep **7**(1): 12465.

Yoshikane, T. and F. Kimura (2005). "Climatic features of the water vapor transport around east Asia and rainfall over Japan in June and September." Geophysical research letters **32**(18).

Zhao, Q., X. Ma, W. Yao and Y. Yao (2019). "A New Typhoon-Monitoring Method Using Precipitation Water Vapor." Remote Sensing **11**(23): 2845.

Zhao, Q., Y. Yao and W. Yao (2018). "GPS-based PWV for precipitation forecasting and its application to a typhoon event." Journal of Atmospheric and Solar-Terrestrial Physics **167**: 124-133.